Measurement and calculation of absolute single- and double-charge-exchange cross sections for O^{6+} ions at 1.17 and 2.33 keV/u impacting He and H$_2$

J. R. Machacek,[1] D. P. Mahapatra,[1] D. R. Schultz,[2] Yu. Ralchenko,[3] A. Chutjian,[1] J. Simcic,[4] and R. J. Mawhorter[5]

[1]*Atomic and Molecular Physics Group, Jet Propulsion Laboratory, Caltech, Pasadena, California 91109, USA*
[2]*Department of Physics, University of North Texas, Denton, Texas 76203, USA*
[3]*Atomic Spectroscopy Group, National Institute of Standards and Technology, Gaithersburg, Maryland 20899-8422, USA*
[4]*Planetary Surface Instruments Group, Jet Propulsion Laboratory, Caltech, Pasadena, California 91109, USA*
[5]*Department of Physics and Astronomy, Pomona College, Claremont, California 91711, USA*

Absolute single- and double-charge-exchange cross sections for the astrophysically prominent O^{6+} ion with the atomic and molecular targets He and H$_2$ are reported. These collisions give rise to x-ray emissions in the interplanetary medium, planetary atmospheres, and comets as they approach the sun. Measurements have been carried out using the Caltech Jet Propulsion Laboratory electron cyclotron resonance ion source with O^{6+} at energies of 1.17 and 2.33 keV/u characteristic of the slow and fast components of the solar wind. Absolute charge-exchange (CE) data are derived from knowledge of the target gas pressure, target path length, incident ion current, and charge-exchanged ion currents. These data are compared with results obtained using the n-electron classical trajectory Monte Carlo method. The radiative and Auger evolution of ion populations following one- and two-electron transfers is calculated with the time-dependent collisional-radiative code NOMAD using atomic data from the flexible atomic code. Calculated CE emission spectra for 100 Å $< \lambda <$ 1400 Å are reported as well and compared with experimental sublevel spectra and cross sections.

PACS number(s): 34.70.+e, 95.85.Mt, 96.60.Vg

I. INTRODUCTION

Charge exchange (CE) between highly charged ion (HCI) projectiles and neutral atomic and molecular target gases can occur when the projectile is a component of the solar wind [1–4], a stellar wind [5], or the precipitating ions from a planetary magnetosphere [6–8]. The neutral target can be a component of the interstellar medium [9], the interplanetary medium [2,10,11], a cometary atmosphere [4,12,13], the lunar exosphere [2], or the rich variety of solar-system planetary atmospheres [3,14].

The fact that x rays are produced in the CE process is of considerable importance since a cold plasma can now become an important source of energetic photons that provide a spectral signature of the projectile ion and a marker for the existence of a cool gas. Cross sections for this exchange are typically large, approximately 10^{-15} cm^2 for the first transfer, and dropping by about a factor of 5 for each subsequent transfer. On the other hand, electron-impact excitation of an x-ray-emitting level in an HCI proceeds with a cross section of $\sim 10^{-18}$ cm^2, or one-thousandth that of CE. Hence, CE becomes a sensitive marker for the presence of the HCI and of the neutral gas environment of a comet, planetoid, and planetary exospheres and atmospheres, the interplanetary medium, the interstellar medium, or circumstellar clouds. Further, the photon emission following CE, mapped spatially and/or temporally by observations, can be used to constrain models of the astrophysical environment yielding profiles of gas density, temperature, and species, for example.

From a theoretical point of view, absolute measurements provide crucial tests of the theories used to describe CE in two ways. First, since calculations can in principle be performed for many more systems than is feasible to measure, measurements can serve to calibrate the reliability of theoretical predictions for systems not considered experimentally but required for the completeness of astrophysical models. Second, and perhaps more importantly, measurements of double- and single-capture cross sections constrain model predictions of photon-emission spectra. The predictions depend on the state-selective capture cross sections both directly via radiative decay and indirectly via autoionization that is highly dependent on the two-electron configurations resulting from double-capture events. Therefore, experiment and theory taken together enable reliable prediction of total cross sections for charge-transfer processes and of the expected emission spectrum.

The electron-capture process for an ion A^{q+} and atomic or molecular target X can be written in a general form as

$$A^{q+} + X \rightarrow [A^{(q-i)+}]^* + X^{i+} \tag{1a}$$
$$\rightarrow [A^{(q-j)+}]^* + X^{k+} + (k-j)e^-$$
$$+ \hbar\omega_1 + \hbar\omega_2 + \cdots + \hbar\omega_n, \tag{1b}$$

where X is the target atom or molecule, $k-j$ is the number of autoionized electrons e, and $\hbar\omega_n$ are the energies of the emitted photons. In total, the target X has supplied k electrons, with j going to the projectile A^{q+} and $k-j$ appearing as autoionized electrons from A and X. For an HCI, simple one-electron transfer occurs to a high n state of A^{q+} that then stabilizes through a series of photon decays. For two- or three-electron transfers (or higher numbers of transfer from multielectron targets), one, two, or three (or more) electrons may be in excited states. The ion then stabilizes by autoionization and photon emission. Thus, a single transfer ($k = 1, j = 1$) and an autoionizing double transfer ($k = 2, j = 1$) contribute to the total single-capture cross section $\sigma_{q,q-1}$. Double transfer ($k = 2, j = 2$), single-autoionizing triple capture ($k = 3, j = 2$), and double-autoionizing quadruple capture ($k = 4, j = 2$) contribute to the double-capture cross section $\sigma_{q,q-2}$, etc. Therefore, a reliable theoretical determination

of the capture cross sections should include a large-scale time-dependent calculation of the radiative-Auger stabilization taking into account all relevant atomic states.

Presented herein are absolute CE cross sections for the projectile O^{6+} ion interacting with He and H_2 targets. The O^{6+} ion was selected since it is the most abundant heavy species (i.e., with mass greater than that for electrons, protons, and α particles, which are the absolute most abundant species) in the solar wind [15] and engages in charge exchange in, for example, comets, solar-system planets and planetoids, the heliosphere, the warm-hot interstellar medium [16], and hot stars [17]. The outline of the presentation is as follows: The experimental approach is given in Sec. II, the theoretical methods using the classical trajectory Monte Carlo approach are presented in Sec. III, results with discussion are found in Sec. IV, and a summary and conclusions are given in Sec. V.

II. EXPERIMENTAL APPROACH

The present measurements were carried out using the electron cyclotron resonance (ECR) ion source and the CE beamline at the Caltech Jet Propulsion Laboratory highly charged ion facility. Mass-selected O^{6+} ions produced in the ECR ion source are extracted at the desired energy before being deflected into the CE beamline. Details of the experimental setup including the beamlines, the CE geometry (effective length of gas cell and entry and exit aperture sizes), and system calibration have been reported elsewhere [18–22]. A brief description is presented below.

The O^{6+} ions produced in the ECR were momentum analyzed in a double-focusing 90° bending magnet and electrostatically deflected through 45° to enter the CE beamline. An einzel lens was used to focus and collimate the beam through a set of three apertures into a target gas cell. The ions undergo CE collisions in the gas cell to produce an ensemble of lower charge states. The ion currents following the CE process were measured in a deep Faraday cup placed at the end of the CE cell. The currents for different charge states were measured sequentially through the application of retarding potentials, the values of which depend on the incident ion energy and charge state. A capacitance manometer (CM) was used to measure the target gas pressure. A schematic of the arrangement can be found in Ref. [18]. The difference between the total measured current and the currents measured after blocking the highest and then sequentially the lower charge states determines the ion current of the individual charge states. A time sequence of the currents measured by applying different retarding potentials produces a spectrum in the form of a staircase, with the number of steps depending on the charge states present in the ion current reaching the Faraday cup. The cross section for CE to a given charge state was computed knowing the incident ion current together with the gas cell pressure [19].

To extract individual CE ion currents, one can write a particle-conservation equation for the current entering the gas cell in terms of the measured CE currents, together with the background current B, given by

$$\frac{I_0}{q} = \frac{I_1 - I_2}{q} + \frac{I_2 - I_3}{q-1} + \frac{I_3 - I_4}{q-2} + \frac{I_4 - I_5}{q-3} + \cdots + B.$$

(2)

Here I_0/q represents the incident particle current of charge state q ($=6$ here) as measured with no gas in the collision cell. The currents $I_1, I_2, I_3, \ldots$ correspond to those measured in the steps after application of the retarding potentials $V_1, V_2, V_3, \ldots$ used to block currents from charge states $q, q-1, q-2, \ldots$ respectively. The terms on the right-hand side, from left to right, correspond to the number of particles with charge $q, q-1, q-2, q-3, \ldots$, respectively. For the present case a maximum of two electron exchanges are possible. Using three retarding potentials, one can block charge states up to $q-2$. In such a case, Eq. (2) has three terms and the background term B.

The cross section $\sigma_{q,q-n}$ for the exchange of n electrons is then given in terms of the experimentally measured parameters as

$$\sigma_{q,q-n} = \frac{kT}{PL} \ln \left(\frac{1}{1 - R_{q,q-n}} \right).$$

(3)

Here T is the target gas temperature, P is the gas pressure, L is the effective gas cell length, and $R_{q,q-n}$ is the particles current ratio given by

$$R_{q,q-n} = \frac{q I_{q-n}}{(q-n) I_q}.$$

(4)

Data acquisition and analysis

All measurements were carried out with $^{18}O_2$ as the source gas. Test mass spectra taken during the two months of continuous running of the source showed only trace amounts of ^{16}O arising from H_2O in the system. No detectable carbon contamination could be found. This is important since $^{12}C^{4+}$, if present, will interfere with $^{18}O^{6+}$, as both have the same mass-to-charge ratio (amu/q = 3.0). A representative mass scan taken at a 7.0-kV extraction potential is shown in Fig. 1. The $^{18}O^{6+}$ ions (henceforth written as O^{6+}) were extracted at potentials of 3.5 and 7.0 kV, with ion energies of 21.0 keV (1.17 keV/u) and 42.0 keV (2.33 keV/u),
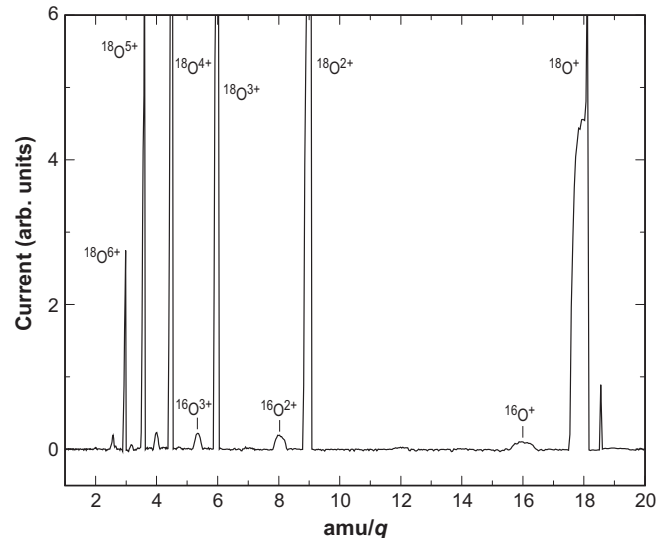

FIG. 1. Mass-charge (amu/q) spectrum of the ECR source for ^{18}O from $^{36}O_2$, with weak features from residual $^{32}O_2$.

TABLE I. Individual and total experimental uncertainties in the O^{6+} charge-exchange measurements with He and H_2.

Source of uncertainty	Uncertainty at the 1σ confidence level (%)
Error in gas density	
capacitance manometer reading	0.3
gas temperature	0.7
pressure reading	2.0
collision cell length	2.0
measurement of beam current	1.0
measurement of CE current ratios	<1.0
Data statistics	
σ_{6-5}	1.0
σ_{6-4}	1.5
systematic errors	1.0
Total error	
σ_{6-5}	3.4
σ_{6-4}	3.6

respectively. These energies correspond to O^{6+} velocities of 474 and 671 km/s, respectively, on the order of the slow (≈ 400 km/s) and fast (≈ 750 km/s) solar-wind velocities. The O^{6+} currents in the measurements were in the range 5–20 nA. All data were acquired at target gas pressures in the range $(6.5 - 12.0) \times 10^{-3}$ Pa, at which no detectable effects of charge exchange involving multiple collisions could be observed.

Three retarding voltages were used for measurement of the CE cross sections $\sigma_{6,5}$ and $\sigma_{6,4}$ for He and H_2. Ion currents were measured in three steps with the last step corresponding to the background level B. The steps were measured by starting with the blocking voltage *off* followed by blocking voltage *on* through the stepwise application of three retarding voltages. In each step ion currents were measured over 125 time intervals for a total sampling time of about 12.5 s, after which the retarding voltage was changed. At a given extraction energy, the retarding potentials V_1, V_2, and V_3 were determined from a variation of the measured ion current with retarding voltage and selecting a suitable value for a given charge state from a zero derivative region. For the case of 7-kV extraction, the retarding potentials for charge states 6+, 5+, and 4+ were 8.0, 9.8, and 11.8 kV, respectively. These potentials were naturally lower for the case with extraction at 3.5 kV.

One cycle of measurement over five steps could be completed in about 1 min with 625 current samples together

with the CM readings. A typical run on a sample usually consisted of 10 cycles collected in about 12 min. To determine the exact gas pressure in the collision cell, *zero runs* on the CM were taken with no gas in the collision cell. These runs were interspersed with the target-gas runs. The CM zero runs taken over a week's time showed a variation 2σ of 1.33×10^{-3} Pa. Total fluctuations in the CM readout never exceeded this limit for the reported measurements.

To obviate slewing-time-related fluctuation in the retarding-potential power supply, 15 data points at the start and 10 data points at the conclusion of the dwell time were discarded in every voltage step. The remaining 100 points in each step were used to determine the current. Cuts were then applied on data points based on correlation plots showing the variation of the measured currents with CM readout and reading of the ion gauge used to measure the vacuum external to the collision cell. Points showing uncorrelated fluctuations were discarded. Remaining data for each rejection voltage were then subjected to a statistical analysis resulting in the determination of the mean values of the currents and their standard errors. These errors, together with the CM error, were used in estimating the statistical errors on the data collected in each cycle. The final cross-section values and their estimated errors for a given sample were obtained by taking the weighted average of data acquired in all the cycles for that sample.

TABLE II. Absolute single- and double-charge-exchange cross sections for the collision of O^{6+} ions with He and H_2. Experimental and theoretical (75% nCTMC and 25% inCTMC initial states) results are shown for the two total ion energies of 21.0 and 42.0 keV. Cross sections are in units of 10^{-15} cm^2, with error limits cited at the 2σ criterion.

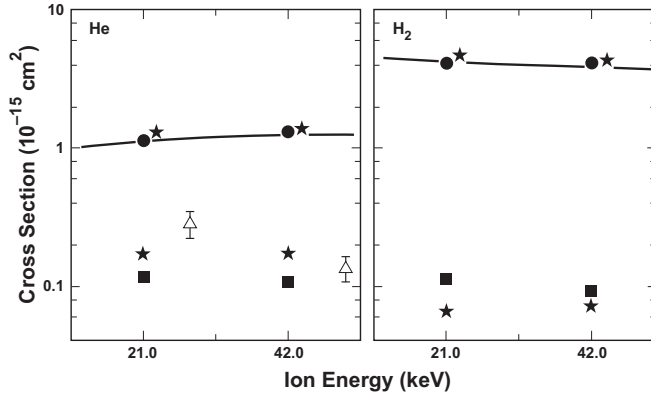|		He		H_2	
	Cross section	21.0 keV	42.0 keV	21.0 keV	42.0 keV
$\sigma_{6,5}$	present experiment	1.16 ± 0.08	1.34 ± 0.09	4.24 ± 0.29	4.24 ± 0.29
$\sigma_{6,5}$	present theory	1.32	1.39	4.64	4.37
$\sigma_{6,4}$	present experiment	0.116 ± 0.008	0.107 ± 0.008	0.118 ± 0.008	0.096 ± 0.007
$\sigma_{6,4}$	present theory	0.173	0.175	0.066	0.073

FIG. 2. Comparison of experimental results with results of calculations from theory (75% *n*CTMC and 25% *in*CTMC initial states). Experimental results are shown for single (●) and double (■) CE of O^{6+} ions with He and H_2 at total ion energies of 21.0 and 42.0 keV. Results of the CTMC calculations are given as stars (⋆), displaced to the right of the single-CE results for clarity. The experimental error bars are smaller than the size of the symbols ● and ■. Also shown are the compiled recommended $\sigma_{6,5}$ results for He and H_2 (——, 24) and other measured values for $\sigma_{6,4}$ [Δ, 25].

A summary of individual and total measurement errors is given in Table I.

The presence of metastable ions in the O^{6+} beam was checked by measuring the CE cross section over a range of ion-source microwave power (50–80 W) with ion-source gas pressure varied in the range $(1.6-2.0) \times 10^{-5}$ Pa, similar to the methods of Refs. [22,23]. No statistically significant variations in CE cross section as a function of ECR parameters were observed. In addition, for one set of ECR parameters, the pressure in the CE gas cell was varied over the range $(1.3-400) \times 10^{-3}$ Pa. The ion current attenuation in the cell was found to be linear, indicating that a single process was dominant. Thus, either the CE cross section for metastable and ground states of O^{6+} are the same or any metastable production was effectively quenched at the ECR source [19].

Further, the pressure in the cell was varied to determine the onset of multiple O^{6+}-gas collisions that would distort partitioning between the single and double exchanges. The cell pressure range $(6.5-12.0) \times 10^{-3}$ Pa was found to be clear of all the above effects. Measurements were carried out at a gas cell pressure of 6.7×10^{-3} Pa. At this pressure the ion-beam attenuation was found to be approximately 2%. Ramping the retarding voltage showed no additional steps, consistent with the absence of CE arising from multiple collisions, in

validation of Eq. (2). A compilation of the measured O^{6+} absolute single- and double-exchange cross sections with He and H_2 at the two ion energies is given in Table II and shown in Fig. 2 along with recommended values for $\sigma_{6,5}$ from an earlier compilation [24] and measurements of $\sigma_{6,4}$ for O^{6+} collisions with He [25]. Shown in Table III are results of single- and double-CE cross sections for O^{q+} ions ($q = 5-8$) with He and H_2 compiled from present results and earlier work in Ref. [18].

III. THEORETICAL APPROACH

Development of the theory leading to total cross sections for single and double capture and prediction of the resulting emission spectra proceeded in three steps. First, the dynamics of the ion-atom or ion-molecule collision was considered using a model that produces a "raw" distribution of states when either a single electron is captured, $O^{6+} + He/H_2 \rightarrow O^{5+} (n\ell)$, or two electrons are captured, $O^{6+} + He/H_2 \rightarrow O^{4+}(n\ell n'\ell')$. Second, autoionization rates for all relevant doubly excited states of the product ion were computed, along with all relevant radiative-decay rates for both singly and doubly excited states so that a radiative-autoionization model could be used to predict how the state, populated in the collision, evolves in the time of passage from the experimental collision regime to the detectors (or in an analogous passage through a low-density gas or plasma). Third, subsequent to the radiative-autoionization processing, the number of events that remained with two electrons captured, or with one, yielded the total cross sections for comparison with experiment. Tracking of the radiative decays during the radiative-autoionization evolution also allowed prediction of the emission spectrum.

The model used to treat the ion-atom or ion-molecule collisions is the classical-trajectory Monte Carlo (CTMC) method [20,21,26–30]. The CTMC model simulates the collision via classical trajectories of the projectile ion (O^{6+}, with the core $1s^2$ electrons taken as inactive), target nuclei, and electrons chosen from an initial ensemble of orbits that mimics the quantum-mechanical electronic binding energy, as well as the radial and momentum distributions of the initial He [26] or H_2 [29,30] targets. This approach gave good agreement with previous measurements in collisions of 7-keVqFe^{q+} ($q = 5-13$) with H_2O [20] and with CO and CO_2 [21].

Two variants of the CTMC method were used, denoted by *n*CTMC and *in*CTMC. The first variant treats the two electrons in He or H_2 as being sequentially bound, an approach that has been shown to provide a good model of the process

TABLE III. Comparison of single- and double-charge-exchange cross sections for O^{q+} ions ($q = 5-8$) with He and H_2 from the present work and Ref. [18]. All values are for 7-keV q total energy, units are 10^{-15} cm^2, and errors are cited at the 2σ error criterion.

	Cross section	O^{5+} Ref. [18]	O^{6+} Present measurements	O^{7+} Ref. [18]	O^{8+} Ref. [18]
He	$\sigma_{6,5}$	1.7 ± 0.2	1.34 ± 0.09	1.8 ± 0.2	2.8 ± 0.4
He	$\sigma_{6,4}$	0.12 ± 0.04	0.107 ± 0.008	0.07 ± 0.06	0.2 ± 0.2
H_2	$\sigma_{6,5}$	2.6 ± 0.3	4.24 ± 0.29	4.5 ± 0.8	5.3 ± 1.0
H_2	$\sigma_{6,4}$	<0.06	0.096 ± 0.007	<0.2	0.7 ± 0.4

of removal of multiple electrons from a target by a highly charged ion [20,21,26]. It reflects the correlation of the initial two-electron target state. The second variant treats the two electrons as being bound by equal amounts (the first ionization potential), as in an independent-electron model, reflecting an uncorrelated initial state, which is typically more applicable for lower charge-state ion-neutral collisions (e.g., H^+ with Ne or Ar). In previous work [20,21], the projectile ion charge state was higher (up to $q = 13$ for Fe vs $q = 6$ for O^{6+}), arguing for use of the nCTMC model. Hence computation of *ab initio* radiative and autoionization rates for the up to fourfold capture of electrons into highly excited states of the complex iron ions was intractable, reducing the sensitivity of the model results to the initial-state representation chosen. In the present case, with the ion charge being lower and calculation of *ab initio* radiative and autoionization rates being much more feasible, a greater sensitivity to the initial-state model was discernible, which allowed adoption of a combination of correlated and uncorrelated initial-state representations, as described below.

Next, the time evolution of states populated in the double- or single-charge-transfer processes was calculated with the collisional-radiative code NOMAD [31]. A total of 4579 $1s^2 n\ell n'\ell'$ levels in O^{4+} with $n \leqslant 7$ and $n' \leqslant 7$ as well as 48 $1s^2 n\ell$ levels in O^{5+} with $n \leqslant 7$ were included in the simulations. The contribution from higher n was neglected since, according to the present CTMC calculations, the charge-transfer cross section into $n > 7$ is typically less than 0.01% of the total cross section. For O^{4+}, most of the included atomic states $1s^2 n\ell n'\ell'$ are above the ionization threshold and can autoionize into O^{5+}. The atomic data required for simulations (i.e., energies and radiative and autoionization probabilities) were calculated with the Flexible Atomic Code (FAC) [32]. The energies of the lowest levels are taken from Ref. [33]. In most laboratory and astrophysical plasmas, the rates of collisional processes are much smaller than the radiative and autoionization probabilities for O^{4+} and O^{5+} and therefore collisions are negligible for stabilization kinetics. This is even more justified for the near-zero target density conditions of the present experiment.

The simulations assumed that the electronic states of O^{4+} and O^{5+} at time $t_0 = 0$ are populated according to the CTMC calculations. Since the CTMC model produces $n\ell$ and $n\ell n'\ell'$ cross sections while our collisional-radiative model is formulated in terms of the fine-structure levels (e.g., of both singlet and triplet nature in O IV), the initial populations of levels were derived from the CTMC cross sections proportional to their statistical weights. The calculation of population evolution was performed on a logarithmic time scale until 10^{-8} s according to the relation $t_1 = 10^{-16}$ s, $t_k = 1.2 t_{k-1}$ for k > 1. Note that a quasisteady state is reached for times on the order of 10^{-10} s, which is a typical lifetime for the strongest radiative transitions in these oxygen ions. Ion flight times from the collision region to detector in the experiment were 600 ± 40 ns (for 3.5 keV q ion energy) and 425 ± 30 ns (for 7 keV q).

Another set of simulations was carried out using relativistic configurations (calculated with the FAC) instead of the fine-structure levels. In this approach, the atomic states are characterized by the total angular momenta of individual electrons rather than by the total angular momentum of all electrons in an ion. Thus, for instance, the 12 levels of the $1s^2 2p3d$ configuration in O^{4+} are represented by the four relativistic configurations $1s^2 2p_\alpha 3d_\beta$, where $\alpha = 1/2$ or $3/2$ for the p electron and $\beta = 3/2$ or $5/2$ for the d electron. These runs showed a much stronger ionization of O^{4+}, with about an order of magnitude larger effective ionization rate than for the atomic-level representation. For the latter, selection rules may suppress some autoionization channels, while for relativistic configurations this is mitigated by the statistical averaging that results in stronger autoionization rates. This effect clearly shows the importance of using fine-structure levels to simulate multielectron-capture stabilization in the radiative-autoionization simulations.

IV. RESULTS AND COMPARISON TO OTHER EXPERIMENTS AND THEORIES

A. Measurement and calculation of total charge-exchange cross sections

Use of the standard CTMC models for O^{6+} ions colliding with He (nCTMC [26]) and H_2 (inCTMC [29,30]) shows reasonably good agreement with measurements. For example, for 7 keV q, nCTMC followed by the radiative-autoionization processing yields a ratio of experimental to theoretical cross sections of 1.11 for single capture and 0.472 for double capture in O^{6+} + He. There is little difference in the ratios for impact at 3.5 keV q. Similarly, for 7-keV q O^{6+} + H_2, the inCTMC plus the radiative-autoionization processing yields experimental-theoretical cross-section ratios of 0.985 for single capture and 1.73 for double capture. From these results one can see that the processed nCTMC results overestimate stable double capture by about a factor of 2, while doing well for single capture, and the processed inCTMC model results underestimate stable double capture by roughly a factor of 2, again doing well for single capture.

Therefore, the measurements, as noted above, indicate that these standard models for He and H_2 may be inadequate to represent the captured $n\ell$ distribution owing to the sensitivity of the autoionization to the captured two-electron states. That is, raw double captures in the nCTMC treatment are likely to have two different principal quantum numbers since the two electrons are initially bound by different ionization potentials (for He, 0.9036 and 1.9998 a.u.). They are therefore quite likely to radiatively stabilize rather than autoionize. In contrast, using the inCTMC model with both electrons initially bound by the same energy (0.9036 a.u.), the resulting double captures are more likely to states with the same principal quantum number and therefore more likely to autoionize. This is borne out by explicit nCTMC and inCTMC calculations and subsequent radiative-autoionization processing. For 7-keV q O^{6+} + He, about 86% of the raw double captures generated by the nCTMC calculation stabilize radiatively, whereas only about 2% do so when generated by the inCTMC calculation. Similarly, for 7-keV q O^{6+} + H_2, the inCTMC calculation produces only 2.6% of the raw double captures that stabilize, while the nCTMC calculation produces almost twice as many. Therefore, the addition of nCTMC and inCTMC initial states

can lower the level of stabilized double captures for He and raise the number for H_2. This leads to better agreement of the theoretical results with measurement and increases the reliability of the predicted emission spectra owing to their dependence on the $n\ell$ distribution of the CE cross sections.

This addition of initial states can be accomplished without recourse to empirical fitting. An accurate quantum-mechanical description of the ground state of He and H_2 can be decomposed into correlated and uncorrelated parts, corresponding to the CTMC initial states chosen assuming correlation (nCTMC, sequential binding energies) or independent electrons (inCTMC, equal binding energies). In particular, He has about 73% correlation and 27% uncorrelated electron motion, while H_2 requires about 80% correlated and 20% uncorrelated electronic wave-function composition. Thus, for simplicity, a model is chosen that includes 75% nCTMC initial states and 25% inCTMC initial states.

The result of this combination of correlated and uncorrelated model initial-state distributions is that for 7-keV

$q\,O^{6+}$ + He the experimental-to-theoretical single-charge-transfer cross section ratio changes from 1.11 to 0.963 and for double charge transfer from 0.472 to 0.611. For 7-keV $q\,O^{6+}$ + H_2 these change from 0.985 for single capture to 0.968 and for double capture from 1.73 to 1.32, showing improvement in both cases for the double-capture ratio without significantly changing the already good agreement with experiment for the single-capture ratios. Thus, the $n\ell$ distributions in both single and double capture are better represented by this hybrid model, as constrained by the measurements. This increases the reliability of not only the total cross sections (Table II) but also the predicted emission spectra.

Magnitudes of these total cross sections are in good agreement with previous measurements. In particular, measurements in Ref. [34] give the total cross section for single-electron capture in 8-keV $q\,O^{6+}$ + He collisions to be $(1.04 \pm 0.28) \times 10^{-15}$ cm^2 and cite earlier work giving a value of $(1.18 \pm 0.18) \times 10^{-15}$ cm^2 [25]. These are to be compared to the present measured result at 7 keV q of $(1.34 \pm 0.09) \times 10^{-15}$ cm^2. Furthermore, the ratio of the single-electron-capture cross section for O^{6+} impact of He to that for H_2 was found to be 0.29 ± 0.04 [34], with a ratio of 0.33 ± 0.07 extracted from earlier work [25,35] for the energy
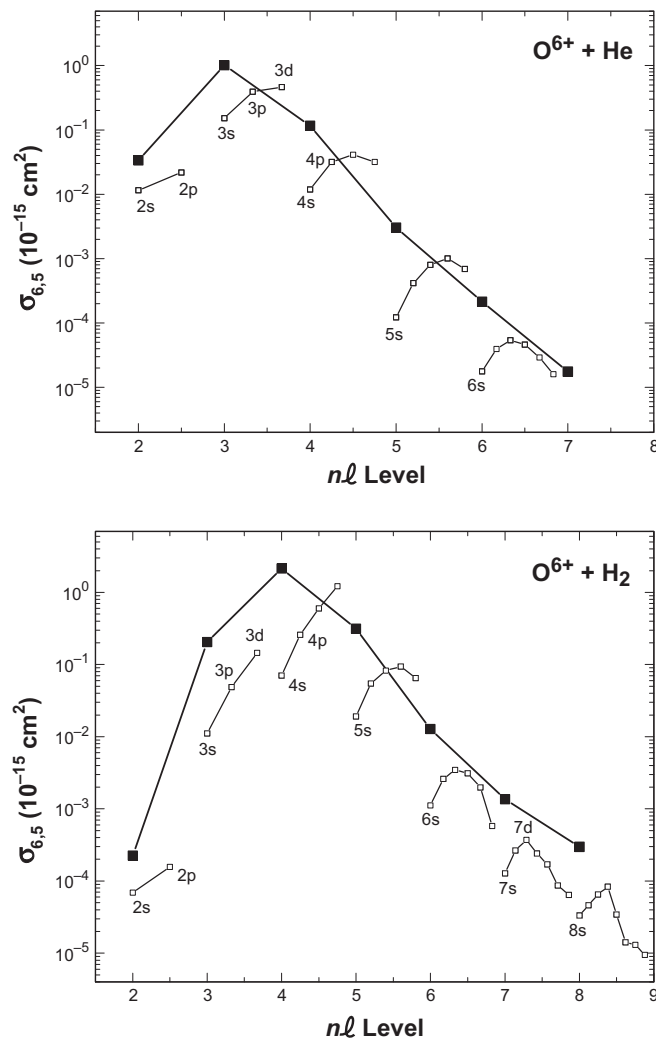

FIG. 3. Raw state-selective single-charge-transfer cross section for He and H_2 produced by the present CTMC model (75% nCTMC and 25% inCTMC initial states) for 7 keV q.
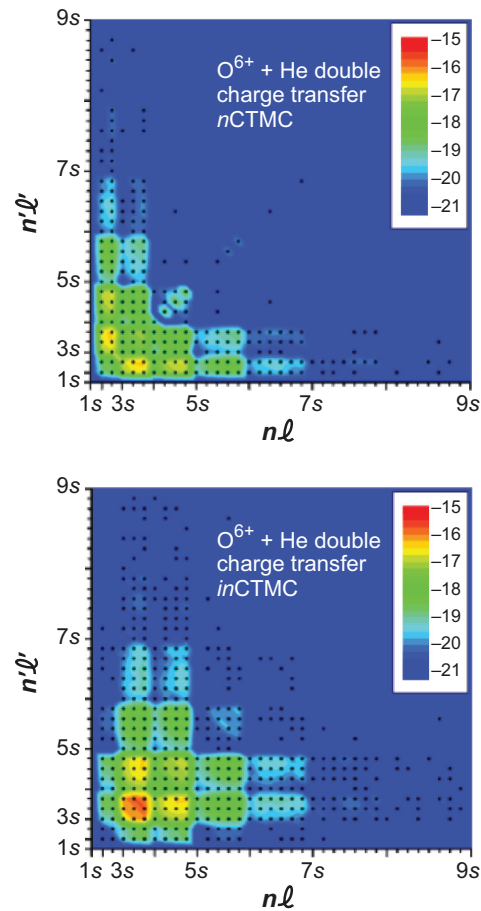

FIG. 4. (Color online) Logarithms of raw state-selective double-charge-transfer cross sections $\sigma_{6,4}$ for He (in units of cm^2) produced in the nCTMC (top) and inCTMC (bottom) models for 7 keV q.
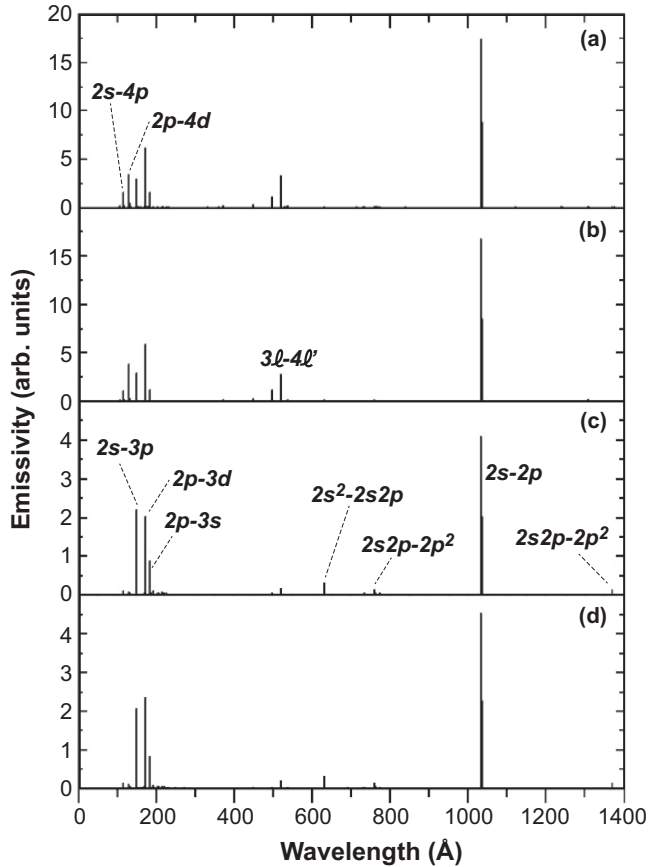
FIG. 5. Predicted emission spectra resulting from single- and double-electron capture with subsequent radiative and autoionizing decay: (a) 3.5-keV q O^{6+} + H_2, (b) 7-keV q O^{6+} + H_2, (c) 3.5-keV q O^{6+} + He, and (d) 7-keV q O^{6+} + He.

considered (8 keV q). A ratio of 0.32 ± 0.03 is found in the present work at 7 keV q.

Calculated, raw, single-capture distributions before radiative-autoionization processing are illustrated in Fig. 3 for 7-keV q O^{6+} + He and H_2 from the model with 75% of the initial states from the nCTMC calculation and 25% from the inCTMC calculation. For He, the distribution as a function of n peaks at $n = 3$, whereas for H_2 it peaks at $n = 4$, reflecting the significant difference in binding energy of the two targets. For higher n levels, the distribution falls off via the well-known Wigner behavior as $1/n^3$. Also shown in

Fig. 3 is the $n\ell$-resolved, raw, single-capture distribution. This distribution peaks at the highest ℓ in each n level for $n \leqslant n_{max}$, as expected [36]. For large n levels, the ℓ distributions peak at successively smaller ℓ values. Nonsmooth variation of the ℓ distributions at large values of n displayed in Fig. 3 reflects the statistical uncertainty in the CTMC simulation for rare (smallest cross section) events. These distributions, along with analogous two-electron-capture states (see Fig. 4), are subsequently processed via the radiative-autoionization model in order to predict theoretical total single- and double-charge-transfer cross sections (Fig. 2) and emission spectra (Fig. 5).

B. Other state-selective measurements of electron capture and results of theories

There is a large experimental and theoretical background to the study of O^{6+} collisions with He and H_2. Spectroscopic measurements have been reported for x-ray [37], vuv [38–43], and visible [44] photon emissions in single charge exchanges. These studies have yielded state-selective electron-capture cross sections that can be compared to the present CTMC results. Also, the production of Auger and Coster-Kronig electrons have been observed in both He [44–48] and H_2 [49] collisions involving double capture by O^{6+}. These experiments have provided evidence for energy and angular correlation effects between the two transferred electrons.

In addition to results of the present CTMC theoretical approach, state-selective cross sections have been calculated by extension of atomic-orbital expansion with close coupling to a two-electron system [50], in a combined *ab initio* approach (for the potential energy curves and couplings) with a semiclassical collision calculation [51], the traveling molecular-orbital method [52], a semiclassical molecular-orbital approximation [53], and the two-center atomic-orbital close-coupling method [54]. Spectroscopic measurements of state-selective cross section for charge transfer have been carried out for several ions, including O^{6+} colliding with He and H_2 in an energy range containing the present impact energies [38]. As shown in Tables IV and V, good experimental-theoretical agreement is found at 3.5 keV q for the $n = 4$ state-selective single-electron-capture cross section for O^{6+} + H_2 [$(2.9-3.0) \times 10^{-15}$ cm^2 from measurements and 2.4×10^{-15} cm^2 from theory]. Good agreement is also found at 7-keV q energy in comparing measurements for single-electron capture to $n = 3$ for O^{6+} + He with the theoretical results [$(1.1-1.3) \times 10^{-15}$ cm^2 from

TABLE IV. State-selective cross sections for single-electron capture in collisions of O^{6+} with H_2. Photon-emission spectroscopic measurements in Ref. [38] are compared with the present theoretical results (75% nCTMC and 25% inCTMC initial states). All cross sections are in units of 10^{-15} cm^2.

H_2	21.0 keV Ref. [40][a]	21.0 keV Ref. [41][a]	21.0 keV Present theory	42.0 keV Ref. [40][a]	42.0 keV Present theory
$n = 4$	3.11	2.87	2.40	2.91	2.10
$4s$	1.22	0.97	0.11	0.91	0.071
$4p$	0.71	0.82	0.38	0.58	0.26
$4d$	0.39	0.37	0.72	0.52	0.60
$4f$	0.78	0.71	1.20	0.90	1.20

[a]Interpolated values from tabulated data.

TABLE V. State-selective cross sections for single-electron capture in collisions of O^{6+} with He. Photon-emission spectroscopic measurements in Refs. [38,39,43] are compared with previous [50] and present theoretical results (75% *n*CTMC and 25% *in*CTMC initial states). All cross sections are in units of 10^{-15} cm^2.

He	21.0 keV Ref. [38][a]	21.0 keV Ref. [39]	21.0 keV Ref. [50][a,b]	21.0 keV Present theory	42.0 keV Ref. [38][a]	42.0 keV Ref. [43][c]	42.0 keV Ref. [50][a,b]	42.0 keV Present theory
$n = 3$	0.96	1.09	1.21	0.98	1.04	1.16	1.29	1.01
$3s$	0.085	0.122	0.145	0.16	0.14	0.17	0.22	0.15
$3p$	0.60	0.661	0.562	0.42	0.63	0.67	0.67	0.39
$3d$	0.28	0.313	0.508	0.40	0.27	0.32	0.41	0.47
$n = 4$	0.20		0.047	0.089	0.21		0.088	0.12
$4s$			0.004	0.0094			0.008	0.012
$4p$	0.069		0.011	0.024	0.039		0.015	0.032
$4d$	0.091		0.024	0.032	0.11		0.042	0.041
$4f$	0.040		0.008	0.024	0.064		0.023	0.032

[a]Interpolated values from tabulated data.
[b]Calculated values from atomic-orbital expansion theory with close coupling.
[c]Interpolated values from figures.

experiment and 1.0×10^{-15} cm^2 from theory]. However, the measurements reveal that the ordering of the ℓ-resolved cross sections within the $n = 4$ shell for H$_2$ and the $n = 3$ and 4 shells for He is not as smoothly varying as predicted by the present theory. This occurs because the details of the quantum-mechanical intermolecular energies, dictating the strength and internuclear radii at which transitions to particular states most likely occur in this low, nearly adiabatic regime, cannot be completely determined for relatively low n levels with high accuracy via the CTMC approach.

For H$_2$, the CTMC method seriously underestimates the $4s$ cross section compared to x-ray measurements of Ref. [40] and predicts an increase in cross section with successively higher angular momentum. Measurements at about 3.5 keV q predict the ordering, from smallest to largest cross section, $4d$, $4f$, $4p$, and $4s$ compared to the CTMC method, which predicts $4s$, $4p$, $4d$, and $4f$. For about 7 keV q, the measured ordering changes to $4d$, $4s$, $4p$, and $4f$ while the CTMC prediction remains $4s$, $4p$, $4d$, and $4f$. For capture to higher n levels, it is likely that the CTMC prediction better reflects reality, but for low n levels, it does not accurately represent the x-ray measurement nor predictions that would come from a more complete quantum-mechanical treatment. For He, the agreement of the CTMC prediction with measurement in ordering and magnitude of the ℓ-resolved cross sections is significantly better, as seen in Table IV. Improvement of the theoretical model would thus necessitate the difficult challenge of carrying out sufficiently complete quantum-mechanical calculations to treat H$_2$ and He involving both single and double charge transfer up to the n levels that significantly contribute to the radiative-Auger cascade.

The raw distribution $n\ell n'\ell'$ of double captures, computed via the nCTMC and inCTMC methods, are illustrated for 7-keV q O^{6+} + He in Fig. 4. These results are shown as plots of $\log(\sigma_{6,4})$ as a function of the two electron configurations $n\ell$ and $n'\ell'$. The distribution resulting from the inCTMC simulation has a strong peak along the diagonal of this plot, particularly around $n = n' = 3$, which indicates the high likelihood of autoionization. In contrast, the nCTMC simulation, with sequential initial electronic binding energies,

shows off-diagonal peaks, thus representing much more asymmetry in the $n\ell n'\ell'$ distribution and therefore the lower likelihood of autoionization. As described above, taking the distribution resulting from 75% nCTMC initial states and 25%
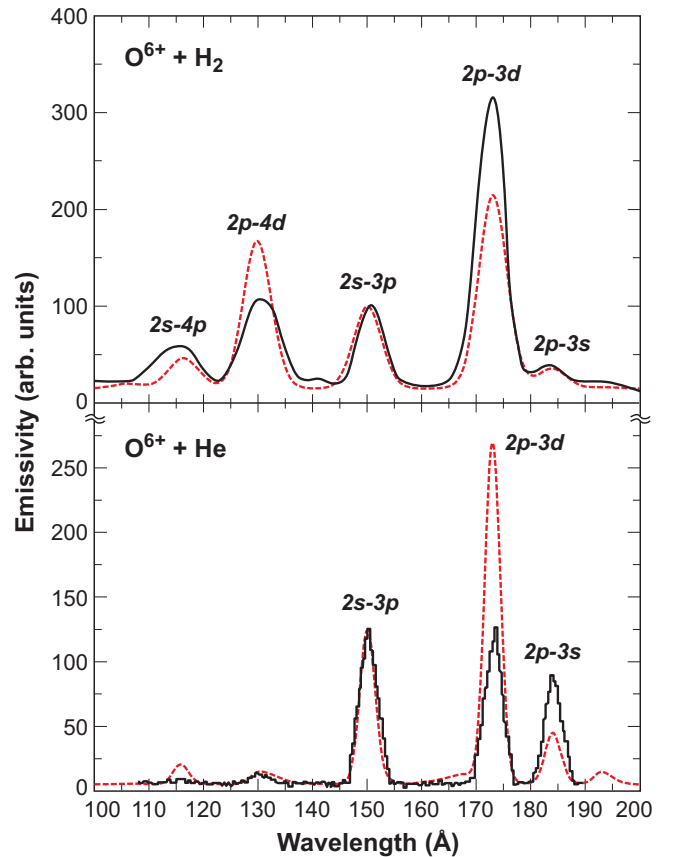

FIG. 6. (Color online) Comparison of the present calculated state-selective emission spectra for O^{6+} CE collisions, the experimental results for H$_2$ [38] at 6.2 keV/u, and the experimental results for He [43] at 4.5 keV/u. Solid curves are the experimental emission spectra and dashed (red) curves are the results of the present theory.

*in*CTMC initial states, reflecting the quantum-mechanical level of correlated and uncorrelated electron motion, yields an asymptotic population (in distance, or in time after the state-populating collision) of radiative decays and autoionization in good agreement with the present measurements of single and double CE. The most prominent lines in the emission spectra, as obtained from the radiative-autoionization processing of the raw CTMC single- and double-capture events, are shown in Fig. 5 for 3.5- and 7-keV q O^{6+} + He and H_2. Tabulations of the full spectra are available from the authors.

Shown in Fig. 6 are comparisons of the calculated x-ray spectra with measured emissions in $O^{6+}-H_2$ [38] and O^{6+}-He [43] charge-exchange reactions at collision energies of 6.2 and 4.5 keV/u, respectively. Since both experimental sets of spectra are reported in arbitrary units of intensity, the calculated spectra were rescaled and a constant background was added to provide the best match with the measurements. Although one can see differences between theory and experiments (e.g., in line-intensity ratios), the general agreement is satisfactory. This provides additional confidence in the CTMC cross sections and the radiation-autoionization kinetics model used therein as well in the experimental results [38,43].

V. CONCLUSION

The present work has provided measurements of total absolute cross sections for single and double capture, which are relevant to plasma and gaseous environments, and has thereby strenuously tested theoretical models seeking to describe these results. It has applicability to a broader range of collisions, not all of which can be comprehensively investigated experimentally. The measurements in turn have constrained the models' predictions of the state-selective cross sections because of the sensitive dependence of autoionization on the $n\ell n'\ell'$ distribution of double capture. With this constraint it is found that one requires autoionization rates that are computed at the fine-structure level and that one should treat the initial ensemble of electronic orbits in the CTMC approach as a hybrid of correlated (nCTMC, sequential binding energies) and uncorrelated (inCTMC, equal binding energies) models. These tests and constraints thereby increase the reliability of measured and predicted emission spectra of interest in plasma and astrophysical simulations due to improved reliability of both the resulting total and state-selective cross sections.

[1] V. Krasnopolsky, Icarus **128**, 368 (1997).

[2] I. P. Robertson, S. Sembay, T. J. Stubbs, K. D. Kuntz, M. R. Collier, T. E. Cravens, S. L. Snowden, H. K. Hills, F. S. Porter, P. Travnicek, J. A. Carter, and A. M. Read, Geophys. Res. Lett. **36**, L21102 (2009).

[3] K. Dennerl, C. M. Lisse, A. Bhardwaj, D. J. Christian, S. J. Wolk, D. Bodewits, T. H. Zurbuchen, M. Combi, and S. Lepri, Astron. Nachr. **333**, 324 (2012).

[4] I. Ewing, D. J. Christian, D. Bodewits, K. Dennerl, C. M. Lisse, and S. J. Wolk, Astrophys. J. **763**, 66 (2013).

[5] J. Liu, S. Mao, and Q. D. Wang, Mon. Not. R. Astron. Soc. **415**, L64 (2011).

[6] Y. Hui, D. R. Schultz, V. A. Kharchenko, P. C. Stancil, T. E. Cravens, C. M. Lisse, and A. Dalgarno, Astrophys. J. **702**, L158 (2009).

[7] Y. Hui, D. R. Schultz, V. A. Kharchenko, A. Bhardwaj, G. Branduardi-Raymont, P. C. Stancil, T. E. Cravens, C. M. Lisse, and A. Dalgarno, J. Geophys. Res. **115**, A07102 (2010).

[8] N. Ozak, D. R. Schultz, T. E. Cravens, V. Kharchenko, and Y.-W. Hui, J. Geophys. Res. **115**, A11306 (2010).

[9] R. Lallement, Space Sci. Rev. **143**, 427 (2009).

[10] I. P. Robertson, and T. E. Cravens, J. Geophys. Res. **108**, 8031 (2003).

[11] S. L. Snowden, M. R. Collier, and K. D. Kuntz, Astrophys. J. **610**, 1182 (2004).

[12] S. J. Wolk, C. M. Lisse, D. Bodewits, D. J. Christian, and K. Dennerl, Astrophys. J. **694**, 1293 (2009).

[13] D. J. Christian, D. Bodewits, C. M. Lisse, K. Dennerl, S. J. Wolk, H. Hsieh, T. H. Zurbuchen, and L. Zhao, Astrophys. J. Suppl. Ser. **187**, 447 (2010).

[14] I. P. Robertson, T. E. Cravens, D. G. Sibeck, M. R. Collier, and K. D. Kuntz, Astron. Nachr. **333**, 309 (2012).

[15] N. A. Schwadron and T. E. Cravens, Astrophys. J. **544**, 558 (2000).

[16] Y. Yao, J. M. Shull, Q. D. Wang, and W. Cash, Astrophys. J. **746**, 166 (2012).

[17] A. M. T. Pollock, Astron. Astrophys. **463**, 1111 (2007).

[18] J. B. Greenwood, I. D. Williams, S. J. Smith, and A. Chutjian, Phys. Rev. A **63**, 062707 (2001).

[19] I. Čadež, J. B. Greenwood, J. Lozano, R. J. Mawhorter, M. Niimura, S. J. Smith, and A. Chutjian, J. Phys. B **36**, 3303 (2003).

[20] J. Simcic, D. R. Schultz, R. J. Mawhorter, J. B. Greenwood, C. Winstead, B. V. McKoy, S. J. Smith, and A. Chutjian, Astrophys. J. **722**, 435 (2010).

[21] J. Simcic, D. R. Schultz, R. J. Mawhorter, I. Čadež, J. B. Greenwood, A. Chutjian, C. M. Lisse, and S. J. Smith, Phys. Rev. A **81**, 062715 (2010).

[22] R. J. Mawhorter, J. B. Greenwood, A. Chutjian, T. Haley, C. D. Mitescu, and J. Simcic, Phys. Rev. A **84**, 052714 (2011).

[23] S. Hossain, S. S. Tayal, S. J. Smith, J. C. Raymond, and A. Chutjian, Phys. Rev. A **75**, 022709 (2007).

[24] *Atomic Data for Fusion*, edited by R. A. Phaneuf, R. K. Janev, and M. S. Pindzola (Oak Ridge National Laboratory, Oak Ridge, 1987), Vol. 5, Figs. 1-169 (He) and 1-253 (H_2).

[25] D. H. Crandall, Phys. Rev. A **16**, 958 (1977).

[26] R. E. Olson and A. Salop, Phys. Rev. A **16**, 531 (1977).

[27] R. Abrines and I. C. Percival, Proc. Phys. Soc. London **88**, 861 (1966).

[28] R. E. Olson, J. Ullrich, and H. Schmidt-Böcking, Phys. Rev. A **39**, 5572 (1989).

[29] L. Meng, C. O. Reinhold, and R. E. Olson, Phys. Rev. A **40**, 3637 (1989).

[30] L. Meng, C. O. Reinhold, and R. E. Olson, Phys. Rev. A **42**, 5286 (1990).

[31] Yu. Ralchenko and Y. Maron, J. Quant. Spectrosc. Radiat. Transfer **71**, 609 (2001).

[32] M. F. Gu, Can. J. Phys. **86**, 675 (2008).

[33] A. Kramida, Yu. Ralchenko, J. Reader, and NIST ASD Team, *NIST Atomic Spectra Database*, version 5.1 (National Institute of Standards and Technology, Gaithersburg, 2013), available at http://physics.nist.gov/asd

[34] L. D. Gardner, J. E. Bayfield, P. M. Koch, I. A. Sellin, D. J. Pegg, R. S. Peterson, M. L. Mallory, and D. H. Crandall, Phys. Rev. A **20**, 766 (1979).

[35] D. H. Crandall, M. L. Mallory, and D. C. Kocher, Phys. Rev. A **15**, 61 (1977).

[36] R. E. Olson, Phys. Rev. A **24**, 1726 (1981).

[37] M. G. Suraud, S. Bliman, D. Hitz, J.-E. Rubensson, J. Nordgren, J. J. Bonnet, M. Bonnefoy, M. Chassevent, A. Fleury, M. Cornille, E. J. Knystautas, and A. Barany, J. Phys. B **25**, 2363 (1992).

[38] D. Dijkkamp, Yu. S. Gordeev, A. Brazuk, A. G. Drentjell and F. J. de Heer, J. Phys. B **18**, 737 (1985).

[39] J. P. M. Beijers, R. Hoekstra, and R. Morgenstern, Phys. Rev. A **49**, 363 (1994).

[40] D. Dijkkamp, D. Ćirić, E. Vlieg, A. de Boer, and F. J. de Heer, J. Phys. B **18**, 4763 (1985).

[41] G. Lubinski, Z. Juhász, R. Morgenstern, and R. Hoekstra, J. Phys. B **33**, 5275 (2000).

[42] S. Bliman, J. Nordgren, E. J. Knystautas, and M. G. Suraud, J. Phys. B **25**, L435 (1992).

[43] C. J. Liu, R. W. Dunford, H. G. Berry, R. C. Pardo, K. O. Groeneveld, M. Hass, and M. L. Raphaelian, J. Phys. B **22**, 1217 (1989).

[44] H. Watanabe, F. J. Currell, H. Kano, N. Kobayashi, N. Nakamura, S. Ohtani, K. Okazaki, H. Tanuma, and U. I. Safranova, J. Phys. Soc. Jpn. **66**, 3790 (1997).

[45] M. Mack and A. Niehaus, Nucl. Instrum. Methods Phys. Res. Sect. B **23**, 116 (1987).

[46] F. W. Meyer, D. C. Griffin, C. C. Havener, M. S. Huq, R. A. Phaneuf, J. K. Swenson, and N. Stolterfoht, Phys. Rev. Lett. **60**, 1821 (1988).

[47] N. Stolterfoht, C. C. Havener, R. A. Phaneuf, J. K. Swenson, S. M. Shafroth, and F. W. Meyer, Phys. Rev. Lett. **57**, 74 (1986).

[48] J.-Y. Chesnel, F. Frémont, B. Sulik, C. Ruiz-Méndez, H. Merabet, C. Bedouet, X. Husson, M. Grether, and N. Stolterfoht, Nucl. Instrum. Methods Phys. Res. Sect. B **154**, 142 (1999).

[49] J. H. Posthumus and R. Morgenstern, J. Phys. B **23**, 2293 (1990).

[50] W. Fritsch and C. D. Lin, J. Phys. B **19**, 2683 (1986).

[51] M. C. Bacchus-Montabonel and K. Amezian, Int. J. Quantum Chem. **38**, 615 (1990).

[52] N. Shimakura, H. Sato, M. Kimura, and T. Watanabe, J. Phys. B **20**, 1801 (1987).

[53] B. C. Saha and A. Kumar, J. Mol. Struct. **487**, 11 (1999).

[54] Y. Q. Zhao, L. Liu, P. Xue, J. G. Wang, and R. K. Janev, J. Phys. B **43**, 185202 (2010).